

## Superconductivity emerging upon Se doping of the quantum spin liquid 1T-TaS<sub>2</sub>


Izidor Benedičič<sup>1</sup>, Nejc Janša<sup>1</sup>, Marion van Midden<sup>1</sup>, Peter Jeglič<sup>1</sup>, Martin Klanjšek<sup>1</sup>, Erik Zupanič<sup>1</sup>, Zvonko Jagličič<sup>2,3</sup>, Petra Šutar<sup>1</sup>, Peter Prelovšek<sup>1,4</sup>, Dragan Mihailovič<sup>1,4</sup> and Denis Arčon<sup>1,4,\*</sup>

<sup>1</sup>*Institute Jožef Stefan, Jamova c. 39, SI-1000 Ljubljana, Slovenia*

<sup>2</sup>*Faculty of Civil and Geodetic Engineering, University of Ljubljana, Jamova c. 2, SI-1000 Ljubljana, Slovenia*

<sup>3</sup>*Institute of Mathematics, Physics and Mechanics, Ljubljana, Jadranska c. 19, SI-1000, Slovenia*

<sup>4</sup>*Faculty of Mathematics and Physics, University of Ljubljana, Jadranska c. 19, SI-1000 Ljubljana, Slovenia*

 (Received 13 May 2020; revised 10 July 2020; accepted 13 July 2020; published 3 August 2020)

Paradigmatic quantum spin liquid has been in the past closely linked to the high-temperature superconductivity. Here we focus on a layered 1T-TaS<sub>2</sub>, which has recently emerged as a surprising candidate for a quantum spin liquid on a triangular lattice. Upon doping 1T-TaS<sub>2</sub> with Se, the <sup>77</sup>Se nuclear magnetic resonance and <sup>181</sup>Ta nuclear quadrupole resonance data show a remarkable robustness of the quantum spin liquid at low Se doping levels despite the growth of inhomogeneities in the electronic state. A dramatic change in the low-energy electronic excitations are observed in samples with a moderate Se content where the Mott insulating state gives way to a correlated metal and a low-temperature superconductivity. The effects of antiferromagnetic correlations can still be traced in the normal state above the superconducting critical temperature  $T_c = 3.5$  K and may, together with the underlying disorder, account for the large superconducting gap-to- $T_c$  ratio  $2\Delta/k_B T_c \approx 7$  deduced from the scanning tunneling microscopy.

DOI: [10.1103/PhysRevB.102.054401](https://doi.org/10.1103/PhysRevB.102.054401)

### I. INTRODUCTION

Quantum spin liquids (QSL) on geometrically frustrated lattices have been in the last two decades intensively studied as a highly intricate quantum spin state characterized by the lack of long-range magnetic ordering or broken lattice symmetries, by the spectrum of fractional excitations (e.g., spinons) and by various topological orders [1,2]. Layered 1T-TaS<sub>2</sub> [Fig. 1(a)] is the latest, somewhat surprising, candidate to realize the QSL that adds to the short list of systems showing QSL on a triangular lattice [3–6]. For 1T-TaS<sub>2</sub>, the QSL regime has been suggested [7–9] on the triangular lattice of Star-of-David units comprising 13 Ta atoms in the low-temperature commensurate charge density wave (CDW) state below 180 K [10–12]. In scanning tunneling microscopy experiments, the Star-of-David structure [Fig. 1(b)] can be clearly observed as twelve Ta atoms (the so-called  $\beta$  and  $\gamma$  sites) move towards the central Ta atom (the  $\alpha$  site) due to the electron-phonon coupling [10]. Such strong polaronic effects lead to a significant band reconstruction where 12 available Ta *5d* electrons per each unit form bands well below the Fermi energy [11]. The thirteenth unpaired electron in the very narrow band crossing the Fermi energy is then localized on each unit because of the electron correlations [11]. In this low-temperature Mott-insulating state, the charge excitations have a clean  $\sim 0.3$  eV gap in the excitation spectrum observed by scanning tunneling spectroscopy (STS) [13] and angle-resolved photoemission spectroscopy

(ARPES) [14], while the surprisingly small and nearly temperature-independent spin susceptibility [8,15,16] is a signature of gapless spin excitations that may be taken as an indication of a QSL.

Since 1T-TaS<sub>2</sub> is so close to the Mott transition, the proximity of such a transition exposes two important questions on how this influences (i) the QSL and (ii) the nature of the competition between the QSL and the emerging metallic/superconducting state. In the Mott insulating phase charge fluctuations may, in addition to the nearest-neighbor antiferromagnetic exchange, induce higher-order ring exchange interactions that together with the spin-orbit coupling stabilize QSL over the competing valence bond solid and the 120° antiferromagnetic order [9]. In such a case, the effective two-dimensional XXZ spin-1/2 model indeed predicts a gapless QSL with a spinon Fermi surface [9]. On the other hand, experimental evidence on the precise nature of QSL in 1T-TaS<sub>2</sub> is not yet conclusive. Previous measurements of <sup>181</sup>Ta spin-lattice relaxation rate,  $1/T_1$ , found a characteristic power-law temperature dependence  $1/T_1 \propto T^\lambda$  with  $\lambda \approx 2$  for temperatures higher than  $T_f = 50$  K and  $\lambda \approx 4$  for  $T < T_f$  [8]. Similar power-law temperature dependencies of  $1/T_1$  were measured previously on several triangular-lattice antiferromagnets realizing the QSL [17–19] and were proposed to arise from the spinon excitations that have nodes in *q* space. On the other hand, the nonzero linear-temperature specific heat coefficient and the finite residual linear term of the thermal conductivity at low temperatures demonstrate the presence of highly mobile gapless excitations [16,20] and thus imply the spinon Fermi surface in agreement with a theoretical prediction [9]. Finally, the extreme broadening in

\*denis.arcon@ijs.si

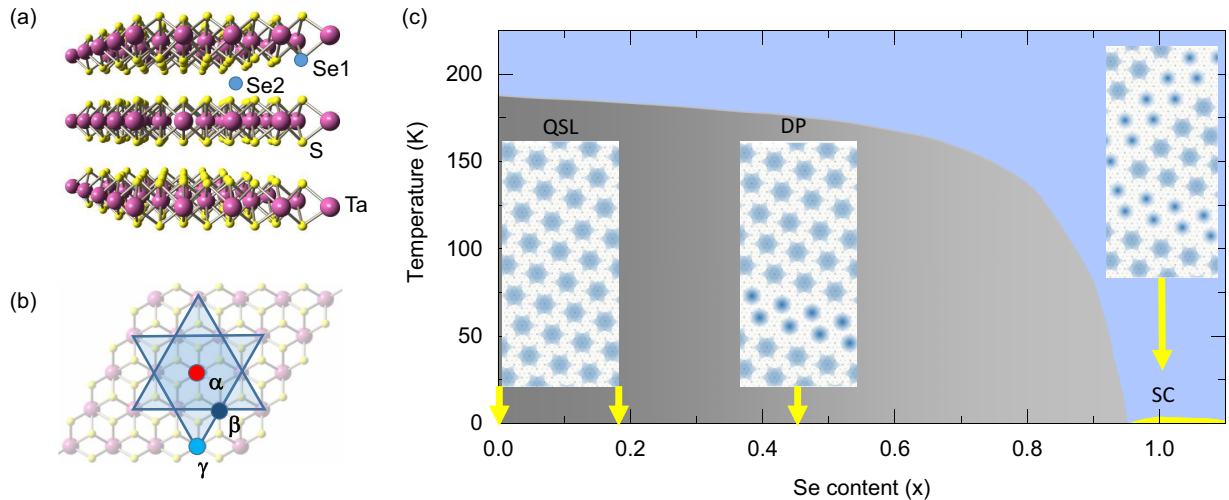


FIG. 1. (a) With doping, Se atoms can enter the layered 1T-TaS<sub>2</sub> structure into two inequivalent sites. They can either substitute a sulfur atom inside a layer (marked as Se1) or intercalate between the layers (marked as Se2). (b) Tantalum atoms that form a Star-of-David occupy three inequivalent sites, denoted as  $\alpha$  (red circle),  $\beta$  (blue circle), and  $\gamma$  (light blue circle) sites. (c) The proposed phase diagram of Se-doped 1T-TaS<sub>2</sub> where the boundary between the nearly commensurate CDW (blue) and commensurate CDW (gray) is obtained from the sudden increase in the in-plane resistivity (adopted from Ref. [26]). The shading denotes the growth of electronic inhomogeneities with increasing Se content  $x$ . The yellow area marks the superconducting dome. Yellow arrows indicate the compositions studied in this work. In the insets, the arrangements of star-of-David units and the domain walls (circles) are schematically shown for the QSL, domain phase (DP), and superconducting (SC) phases for different Se-doping levels.

the distribution of  $1/^{181}\text{T}_1$  below  $T_f$  [8] highlights the possible importance of disorder in the realistic 1T-TaS<sub>2</sub> material that may alternatively promote the bond randomness-induced QSL [21–23] or may even stabilize a valence-bond glass [24].

It is truly remarkable that the application of very different control parameters leads to qualitatively similar phase diagrams of 1T-TaS<sub>2</sub>—commensurate CDW with QSL gives way to superconductivity with a domelike dependence of the critical temperature  $T_c$  on the control parameter [Fig. 1(c)]. Specifically, low-temperature superconductivity with  $T_c \approx 5$  K has been reported when 1T-TaS<sub>2</sub> has been exposed to pressures higher than 3 GPa [12], upon substitution of S with the chemically similar Se [25] leading to changes in the orbital texture and the Mottness collapse [26] or by Fe doping where the control of the TaS<sub>2</sub> layer charge state is achieved [27]. These results point to the fragility of the parent QSL against external perturbation and question the role of disorder in the formation of QSL and the competing superconducting state, the nature of the normal metallic state from which superconductivity develops, and lastly the nature of the superconducting state itself.

In order to throw light on these questions, we report here a comparative local-probe  $^{181}\text{Ta}$  nuclear quadrupole resonance (NQR),  $^{77}\text{Se}$  nuclear magnetic resonance (NMR), and scanning tunneling microscopy (STM) study of pristine and Se doped 1T-TaS<sub>2</sub>. Present results suggest the importance of disorder in the low-temperature ground state and the remnant of antiferromagnetic fluctuations in the normal metallic state upon Mottness collapse. Both factors must be considered to explain the large superconducting gap-to- $T_c$  ratio  $2\Delta/k_B T_c \approx 7$  and provide new insights into the interplay between frustrated magnetism and superconductivity in strongly-correlated electron systems.

## II. EXPERIMENTAL DETAILS

For NQR and NMR experiments, powder samples of Se-doped 1T-TaS<sub>2</sub> were used. We have used a two-stage synthesis procedure. A stoichiometric amount of tantalum and selenium was put into a quartz ampule with a small excess of selenium. The mixture was sealed and heated to 900 °C for four days and then quenched in cold water. In the second stage sulfur and tantalum were added to achieve targeted stoichiometry ratios and then heated to 950 °C for 10 days before quenching again in cold water. The doping level was monitored using energy-dispersive x-ray spectroscopy.

Zero-field  $^{181}\text{Ta}$  (nuclear spin  $I = 7/2$ ) NQR measurements were performed on crystal samples, grown from the powder using a chemical vapor transport method [8]. Measurements were made at temperatures between 5 K and 180 K in a continuous-flow liquid-He cryostat. Similarly as in our previous measurements [8], several thin single crystals were carefully stacked and placed into a NMR sample holder. Inversion recovery nuclear magnetization curves were analyzed using an appropriate model for the spin-lattice relaxation of a nuclear spin  $I = 7/2$ , irradiated at the  $1/2 \leftrightarrow 3/2$  NQR transition:

$$m_z(\tau) = A[1 - 0.024e^{-(3\tau/T_1)^p} - 0.235e^{-(10\tau/T_1)^p} - 0.741e^{-(21\tau/T_1)^p}] + B. \quad (1)$$

Here  $A$  and  $B$  are the constants related to the initial and  $\tau \rightarrow \infty$  values of the  $^{181}\text{Ta}$  magnetization, and  $p$  is a stretching exponent that simulates the distribution of  $1/T_1$  values.

$^{77}\text{Se}$  (nuclear spin  $I = 1/2$ ) NMR experiments were performed in 9.39 T magnetic field at temperatures between 6 K and 160 K in a continuous-flow liquid-He cryostat. In this field, the  $^{77}\text{Se}$  NMR reference frequency is

${}^{77}\nu_{\text{rf}} = 76.282$  MHz.  ${}^{77}\text{Se}$  NMR spectra were recorded using a standard Hahn-echo  $\pi/2$ - $\tau$ - $\pi$ - $\tau$  pulse sequence with an interpulse delay  $\tau = 100$   $\mu\text{s}$  and an optimized  $\pi$  pulse length of 6  $\mu\text{s}$ . Since the excitation bandwidth of pulses was smaller than the NMR line width, we measured Hahn-echo signal at multiple frequencies in steps of 50 kHz and the wide-line NMR spectra were then reconstructed from the summation of partial NMR spectra.

${}^{77}\text{Se}$  spin-lattice relaxation measurements were carried out using an inversion recovery pulse sequence  $\pi$ - $\tau$ - $\pi/2$ - $t_D$ - $\pi$ - $t_D$  with  $t_D = 100$   $\mu\text{s}$  and a variable delay  $\tau$ . Spin-lattice relaxation rates,  $1/T_1$ , were extracted by fitting  ${}^{77}\text{Se}$  magnetization curves to

$$m_z(\tau) = A(1 - e^{-(\tau/T_1)^p}) + B, \quad (2)$$

where  $A$ ,  $B$ , and  $p$  have a similar meaning as in the case of  ${}^{181}\text{Ta}$  NQR study.

For the low temperature STM measurements, single crystals were grown using a standard chemical vapor transport method with iodine as a transport agent. After cleaving in ultra-high-vacuum (UHV) at room temperature, the samples were transferred to a Specs JT-STM with a base temperature of 1.2 K. Measurements were performed using etched W tips characterized on a clean Ag(111) surface. Topography images were taken in constant current mode and the  $dI/dV$  spectra were taken with a standard lock-in technique with a modulation frequency  $f = 733$  Hz and a modulation amplitude 100  $\mu\text{V}$ , unless stated otherwise.  $dI/dV$  measurements with setpoint parameters  $I_t = 1.2$  nA and  $V_{\text{setpoint}} = 20$  mV were performed at temperatures of 1.2 K and 10 K on a 5 nm  $\times$  5 nm spatial grid.

### III. RESULTS

#### A. ${}^{181}\text{Ta}$ NQR on 1T-TaS<sub>2</sub> with low Se doping

Just like in pristine 1T-TaS<sub>2</sub> [8,28,29], the  ${}^{181}\text{Ta}$  NQR spectrum of a sample with the low Se doping, i.e., with the composition of 1T-TaS<sub>1.82</sub>Se<sub>0.18</sub>, consists of a resonance centered around 79.6 MHz [Fig. 2(a)], which is attributed to the Ta  $\alpha$  sites, and a broad resonance around 100 MHz [inset to Fig. 2(a)], where the individual lines of Ta  $\beta$  and  $\gamma$  sites significantly overlap. The observation of separate  $\alpha$  and  $\beta/\gamma$   ${}^{181}\text{Ta}$  NQR signals demonstrates that the light Se doping of 1T-TaS<sub>2</sub> does not disrupt the formation of the Star-of-David Ta units in the commensurate CDW state. The temperature dependence of the NQR frequency,  $\nu_Q$ , in Se-doped sample for the  $\alpha$  site [Fig. 2(b)] still shows a smooth and monotonic temperature dependence and is very similar to that of the pristine 1T-TaS<sub>2</sub>. We thus conclude that low Se doping does not lead to any structural or electronic instabilities of commensurate CDW.

However, the introduction of Se does lead to a considerable broadening of the  ${}^{181}\text{Ta}$  NQR lines compared to pristine 1T-TaS<sub>2</sub> [Fig. 2(a)]. The line-broadening mirrors the increased distribution in the  ${}^{181}\text{Ta}$  quadrupole frequencies induced by the local structural disorder and strain as Se starts to randomly populate S sites in the Star-of-David units [(Fig. 1(b)]. At the lowest temperature reached in these experiments,  $T = 4$  K,  ${}^{181}\text{Ta}$  NQR spectrum of the Se-doped sample, besides the Se

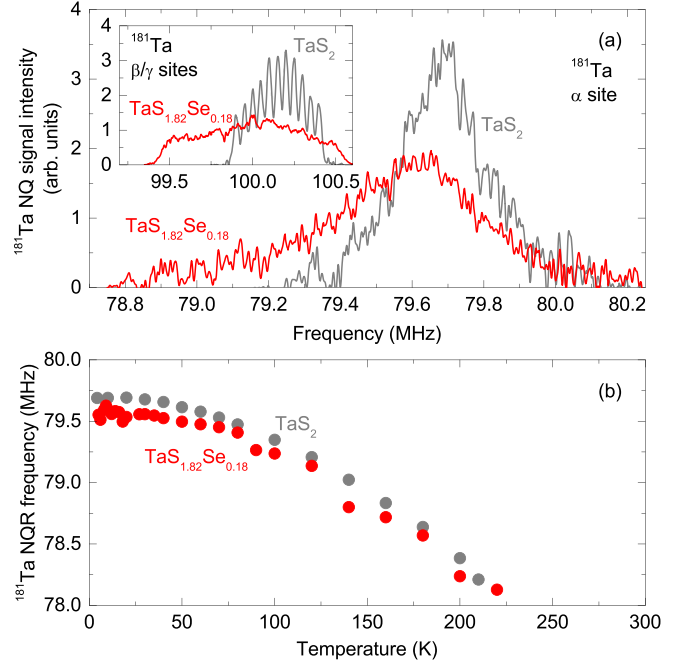


FIG. 2. (a) Comparison of  ${}^{181}\text{Ta}$  NQR spectra measured on the  $\alpha$  site in 1T-TaS<sub>2</sub> (gray line) and 1T-TaS<sub>1.82</sub>Se<sub>0.18</sub> (red line) samples. Inset: The corresponding  ${}^{181}\text{Ta}$  NQR spectra for the  $\beta$  and  $\gamma$  sites. All spectra were taken at  $T = 20$  K. (b) Temperature dependencies of the  ${}^{181}\text{Ta}$  NQR frequencies for the  $\alpha$  site in 1T-TaS<sub>2</sub> (gray circles) and 1T-TaS<sub>1.82</sub>Se<sub>0.18</sub> (red circles) samples, respectively.

site-disorder induced, does not show any additional broadening that could be associated with the onset of any static long- or short-range magnetism and therefore the putative QSL initially appears resilient against Se doping.

To prove the presence of the QSL experimentally, one needs to focus on the detection of fractional spinon excitations, which are one of the defining properties of QSL. In the NQR experiment, the low-energy part of the spectrum of spinon excitations governs the temperature dependence of the spin-lattice relaxation rates,  $1/T_1$ . In the case of 1T-TaS<sub>1.82</sub>Se<sub>0.18</sub>, the temperature dependence of  ${}^{181}\text{Ta}$   $1/T_1$  for the  $\alpha$  site can be divided into three temperature regimes (Fig. 3): The high-temperature regime in the metallic nearly commensurate CDW phase ( $T > 160$  K) where  $T_1$  is extremely short (for example, at  $T = 200$  K we obtain  $T_1 = 1.9$  ms) and thus very difficult to measure at higher temperatures where it gets even shorter, the intermediate temperature regime between  $\sim 20$  K and 160 K already within the commensurate CDW phase that is characterized by the power-law dependence  $1/T_1 \propto T^\lambda$  with  $\lambda \approx 2.7$ , and the low-temperature regime ( $T < 20$  K) where the variation of  $1/T_1$  with temperature is much less pronounced as it adopts a different power-law dependence  $1/T_1 \propto T^\eta$  with a sublinear  $\eta \approx 0.6$ .

Such temperature dependence of  ${}^{181}\text{Ta}$   $1/T_1$  resembles that of the pristine 1T-TaS<sub>2</sub> (Fig. 3) for which it has been taken as a hallmark of the QSL [8]. The similarity extends even further as we also find the stretched exponential  ${}^{181}\text{Ta}$  nuclear magnetization curves with the stretching exponent  $p$  changing from  $p = 1$  at highest temperatures to a very

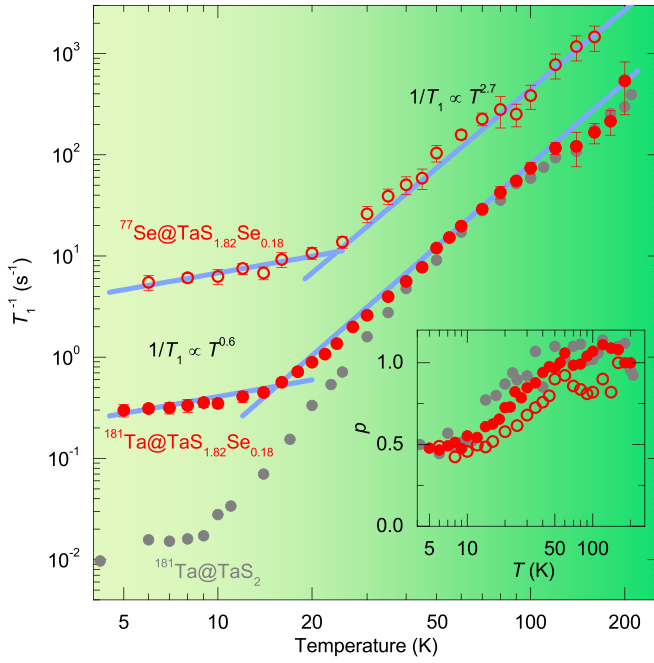


FIG. 3. Temperature dependence of the zero-field  $^{181}\text{Ta}$  spin-lattice relaxation rate,  $1/T_1$ , in pristine  $1\text{T-TaS}_2$  (gray circles) and  $1\text{T-TaS}_{1.82}\text{Se}_{0.18}$  (solid red circles) for the  $\alpha$  site. For comparison, the temperature dependence of  $^{77}\text{Se}$   $1/T_1$  (open red circles) for  $1\text{T-TaS}_{1.82}\text{Se}_{0.18}$  sample is also shown. Solid blue lines represent power-law temperature dependencies  $1/T_1 \propto T^\eta$  with power-law exponents  $\eta = 2.6$  ( $T > 20$  K) and  $\eta = 0.6$  ( $T < 20$  K), respectively. Within the accuracy of these measurements, all temperature dependencies can be described by the same power law exponents. Inset: temperature dependence of stretching exponent,  $p$ , from  $^{181}\text{Ta}$   $1/T_1$  measurements for the pristine  $1\text{T-TaS}_2$  (gray circles) and the  $1\text{T-TaS}_{1.82}\text{Se}_{0.18}$  (red circles) sample. The stretching exponent obtained from the  $^{77}\text{Se}$   $1/T_1$  data on  $1\text{T-TaS}_{1.82}\text{Se}_{0.18}$  is represented by open red circles.

small value of  $p \sim 0.5$  at the lowest temperatures (inset to Fig. 3), which is a signature of a very broad distribution of spin-lattice relaxation rates. However, we also notice two important qualitative differences. First, in the pristine  $1\text{T-TaS}_2$  sample the reduction in the density of low energy excitations below  $T_f = 50$  K is detected by the  $^{181}\text{Ta}$   $\alpha$  site as an increase of the power-law exponent  $\lambda$  from the high-temperature value of 2 to low-temperature  $\sim 4$ . For the lightly Se doped sample, the same power-law exponent  $\lambda \approx 2.7$ , which is somewhere in between the high- and low-temperature values of  $\lambda$  in pristine sample, applies down to  $\sim 10$  K. Se doping thus removes or at least largely broadens the instability that changes the spectrum of low-energy excitations at  $T_f$ .

The second important difference refers to the magnitude of  $^{181}\text{Ta}$   $1/T_1$ . While the high-temperature values of  $1/T_1$  measured for the  $1\text{T-TaS}_{1.82}\text{Se}_{0.18}$  sample coincide with those of the pristine  $1\text{T-TaS}_2$ , the spin-lattice relaxation rates appear significantly enhanced by more than one order of magnitude in the low-temperature sublinear regime for the Se-doped sample (Fig. 3). Therefore, the relaxation mechanism that is responsible for the sublinear temperature dependence of  $1/T_1$  with  $\eta \approx 0.6$  is substantially enhanced by the Se doping.

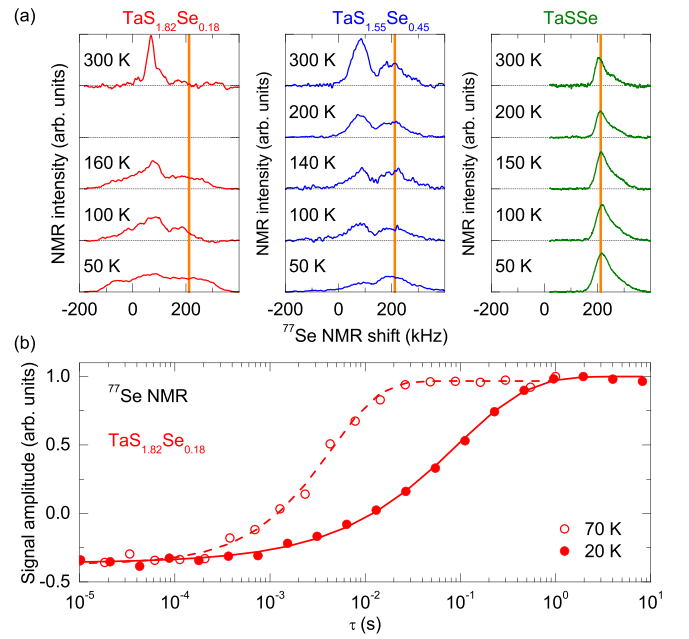


FIG. 4. (a) Comparison of the  $^{77}\text{Se}$  NMR spectra of  $1\text{T-TaS}_{1.82}\text{Se}_{0.18}$ ,  $1\text{T-TaS}_{1.55}\text{Se}_{0.45}$ , and  $\text{TaSSe}$  samples. The  $^{77}\text{Se}$  NMR shift is measured relative to the reference frequency of  $\nu_{\text{ref}} = 76.282$  MHz in the magnetic field of 9.39 T. Vertical orange line marks the position of the S peak measured in the  $\text{TaSSe}$  sample. (b)  $^{77}\text{Se}$  nuclear magnetization recovery curves for the  $1\text{T-TaS}_{1.82}\text{Se}_{0.18}$  sample measured at 70 K (open red circles) and 20 K (solid red circles). Between 100 K and 20 K the relaxation rate decreases by two orders of magnitude, accompanied by a significant departure of the stretching exponent from 1.

## B. $^{77}\text{Se}$ NMR

In the studies of  $1\text{T-TaS}_2$  samples with higher Se-doping concentrations,  $^{181}\text{Ta}$  NQR measurements proved to be extremely challenging because of a significant NQR line broadening. Selenium atoms that substitute sulfur atoms in the lattice represent an alternative local probe of magnetism in  $\text{TaS}_2$  layers. Unlike  $^{181}\text{Ta}$  NQR signal,  $^{77}\text{Se}$  ( $I = 1/2$ ) NMR signal is expected to become stronger with increased doping, making it thus especially useful for samples with higher Se content. Room temperature  $^{77}\text{Se}$  NMR spectra of Se-doped  $1\text{T-TaS}_2$  samples generally show two distinct peaks [Fig. 4(a)]. The first one, shifted for about  $\Delta\nu = 70$  kHz ( $\delta = \Delta\nu/\nu_{\text{ref}} \approx 900$  ppm) from the  $^{77}\text{Se}$  reference frequency,  $\nu_{\text{ref}}$ , is clearly visible in the low- and moderately-Se doped samples  $1\text{T-TaS}_{1.82}\text{Se}_{0.18}$  and  $1\text{T-TaS}_{1.55}\text{Se}_{0.45}$ , respectively. Such a shift is within the values expected for a chemical shift of  $^{77}\text{Se}$  [30]. Therefore, we label this peak as a “nonshifted” NS peak.  $^{77}\text{Se}$  spin-lattice relaxation time of NS peak is about 10 s at 100 K. Both small shift and its long  $T_1$  imply that the hyperfine coupling of these Se sites to the unpaired moments in  $\text{TaS}_2$  layers is weak. We thus tentatively assign the NS peak to the Se atoms intercalated in between layers [Fig. 1(a)].

The second peak grows in intensity with increasing Se content and is best seen in the  $1\text{T-TaSSe}$  sample. Its large shift (hereafter we will refer to this peak as the shifted S peak) is about  $\Delta\nu = 210$  kHz ( $\delta \sim 2700$  ppm) and thus cannot

be attributed to the  $^{77}\text{Se}$  chemical shift alone. Moreover, its  $T_1 = 2.3$  ms at 100 K and is several orders of magnitude shorter than that of the NS peak. The large shift and short  $T_1$  of the S peak therefore must arise from the significant hyperfine interaction with the unpaired polaron spins of  $\text{TaS}_2$  layer, so we associate this peak with the Se atoms that substitute S atoms inside layers. The absence of a NS peak for the 1T-TaSSe sample is connected with the fact that the stoichiometric composition is chemically more stable.

The temperature dependence of  $^{77}\text{Se}$   $1/T_1$ , measured at the S-peak position in the sample with the lowest Se doping (i.e., the 1T-TaS $_{1.82}\text{Se}_{0.18}$  sample) is shown in Fig. 3 together with the  $^{181}\text{Ta}$  NQR data. At high temperatures,  $^{77}\text{Se}$   $1/T_1$  again follows a power law temperature dependence  $1/T_1 \propto T^\lambda$ . Such dependence with  $\lambda = 2.6 \pm 0.1$  can be clearly observed between 160 K, where the commensurate CDW phase forms and the S peak can first be detected, and  $\sim 20$  K. Below 20 K, the temperature dependence of  $1/T_1$  becomes less pronounced and adopts the sublinear  $1/T_1 \propto T^\eta$ , with  $\eta = 0.55 \pm 0.1$ . Measurements of  $^{77}\text{Se}$  NMR and  $^{181}\text{Ta}$  NQR spin-lattice relaxation rates (Fig. 3) thus yield qualitatively the same temperature dependencies with the same power-law exponents that are indistinguishable within the margin of error. A small difference in the crossover temperature deduced from the  $1/T_1$  data for  $^{181}\text{Ta}$  and  $^{77}\text{Se}$  nuclei may mark the relative difference in the low-temperature contribution to the spin-lattice relaxation. Moreover, for the  $^{77}\text{Se}$  nuclear magnetization relaxation curves [Fig. 4(b)] we observe the change of the stretching exponent  $p$  from  $\approx 0.9$  at  $T > 50$  K to  $\approx 0.5$  at the lowest temperatures, exactly like it is found for  $^{181}\text{Ta}$  NQR data (inset to Fig. 3 and Ref. [8]). These similarities imply that both nuclei probe the same type of low-energy spin excitations. As such power-law dependencies are fingerprints of the QSL, the present data suggests perseverance of the QSL on a star-of-David triangular lattice upon light Se-doping of 1T-TaS $_2$ , whereas  $p \rightarrow 0.5$  at low temperatures highlights the magnetic inhomogeneities as an important intrinsic feature of this state.

The temperature dependence of  $^{77}\text{Se}$   $1/T_1$  for the S peak in the Se-doped samples with higher Se concentrations, i.e., for the 1T-TaS $_{1.55}\text{Se}_{0.45}$  and TaSSe samples, shows a distinctly different behavior when compared to the 1T-TaS $_{1.82}\text{Se}_{0.18}$  sample (inset to Fig. 5). Strikingly, with higher Se-doping concentrations the  $^{77}\text{Se}$  relaxation is severely slowed down—at the lowest temperatures  $1/T_1$  is smaller by almost an order of magnitude. This result not only indicates that the density of spinon excitations in the QSL of the parent 1T-TaS $_2$  must be high but also that the  $^{77}\text{Se}$  hyperfine coupling constant probably changes with the Se concentration too. The latter corroborates the proposed change in the orbital texture as the density of domain walls increases with Se doping [26]. In agreement with the proposed delocalized nature of orbitals dominating at higher Se concentrations [26],  $^{77}\text{Se}$   $1/T_1$  decreases roughly linearly with temperature, which is reminiscent of the Korringa spin-lattice relaxation in metals [31,32]. The existence of metallic-type response in this part of the phase diagram is indicative of the electronic inhomogeneities, probably linked to the growth of mosaicity as indicated in the inset of Fig. 1(c) and directly observed in the low-temperature STM studies [26].

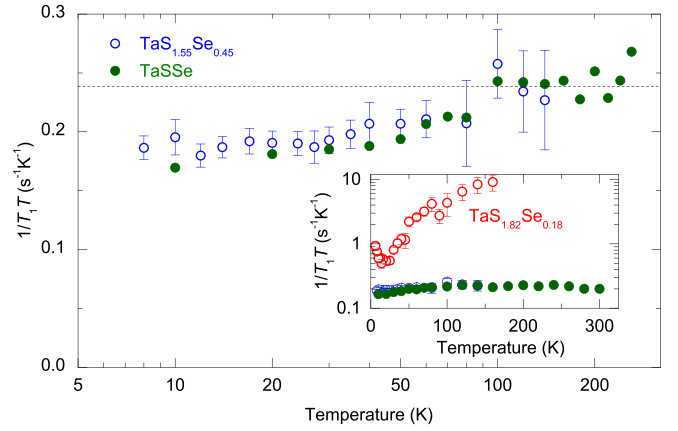


FIG. 5. Temperature dependence of the  $^{77}\text{Se}$  spin-lattice relaxation rate divided by temperature  $1/T_1T$  for the 1T-TaS $_{1.55}\text{Se}_{0.45}$  (open blue circles) and TaSSe (green circles) samples. Both samples exhibit a metallic-type behavior with the Korringa-like relaxation rate given by  $1/T_1T = \text{const.}$  that is slightly suppressed at temperatures below 100 K. The horizontal dashed line marks the high-temperature value of  $1/T_1T$ . Inset: the same data plotted together with  $^{77}\text{Se}$  NMR  $1/T_1T$  of 1T-TaS $_{1.82}\text{Se}_{0.18}$  (open red circles).

Below 100 K, the  $^{77}\text{Se}$   $1/T_1$  gradually slows down and  $1/T_1$  is slightly reduced from the expectations of the Korringa relation  $1/T_1T = \text{const.}$  by about 20% (Fig. 5). In correlated metals, deviations from the Korringa relation are usually attributed to the presence of magnetic fluctuations [32], in this case probably antiferromagnetic fluctuations of the parent QSL state. The effect of magnetic fluctuations is still observable even for TaSSe, where the system is already deep in the metallic nearly commensurate CDW state and where superconductivity is expected to emerge at low temperatures. As the high magnetic fields in these  $^{77}\text{Se}$  NMR experiments completely suppress superconductivity, the nature of the superconducting state that develops from such a correlated metallic state cannot be addressed with NMR.

### C. Superconductivity emerging from the QSL upon Se doping

For the TaSSe sample (the polycrystalline sample was taken from the same batch as used for the  $^{77}\text{Se}$  NMR experiments), measurements of sample's magnetization revealed a bulk diamagnetic response below the superconducting critical temperature of  $T_c = 3.4$  K [Fig. 6(a)]. The superconducting fraction is estimated to be about 20%, which rules out any parasitic phase or filamentary type [33] of superconductivity in this case. We note that the observation of bulk superconducting response agrees well with the literature data, where it was previously reported to develop below  $T_c = 3.5$  K [25].

Additional evidence of superconductivity comes from low temperature STM measurements, which were performed on selected flakes of the TaSSe sample. Topographic images of the TaSSe surface reveal charge density mosaicity consisting of nanometer-sized (typical size is  $< 10$  nm) CDW domains separated by sharp translational and rotational domain walls, as can be seen in Fig. 6(b). We note that such mosaicity is strongly reminiscent of the 1T-TaS $_2$  metallic states induced from the parent Mott insulating state by the external

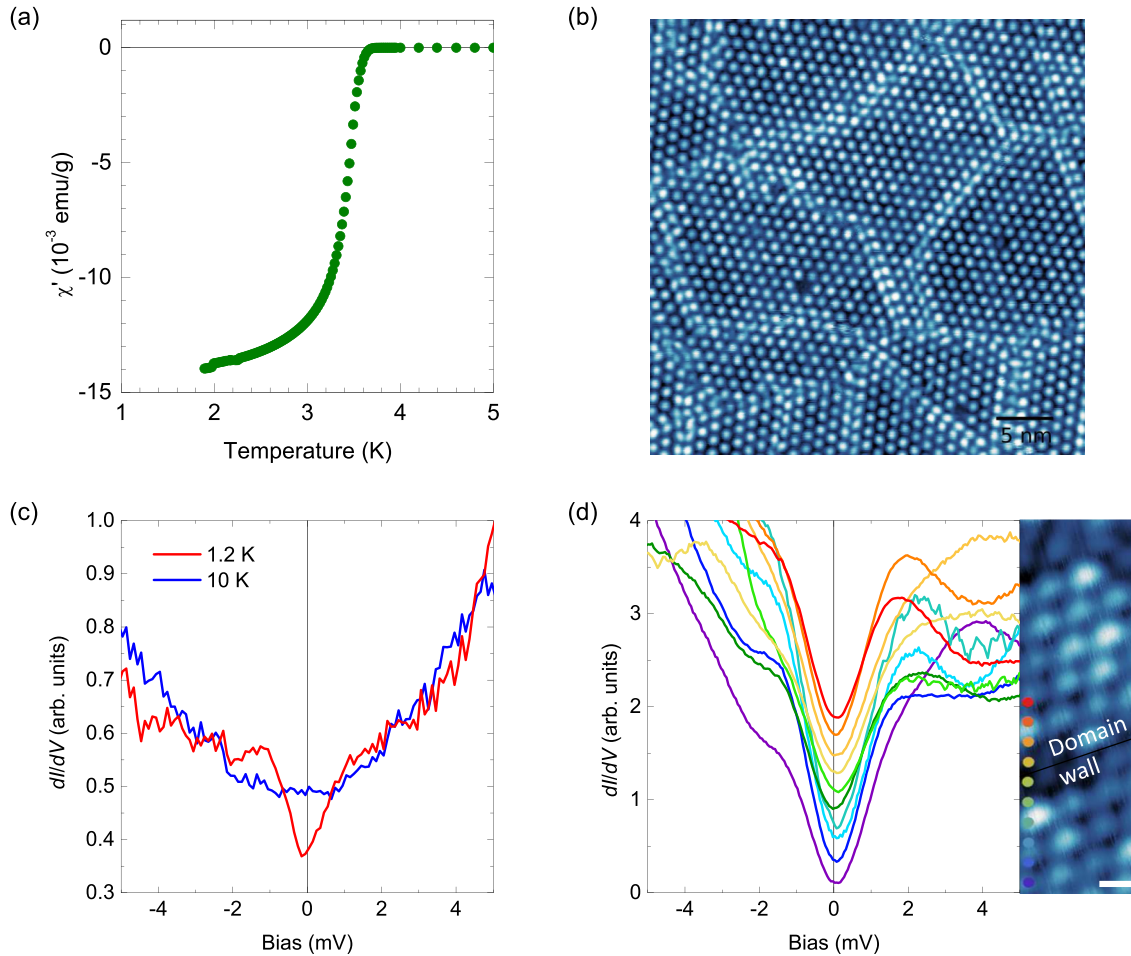


FIG. 6. (a) Temperature dependence of the ac magnetic susceptibility measured in a magnetic field of 0.65 mT for the TaSse sample shows a bulk diamagnetic response below the superconducting critical temperature of  $T_c = 3.5$  K. (b)  $40 \times 40$  nm STM topographic image of cleaved TaSse. The image was taken at 375 mV bias voltage and 82 pA tunneling current. Please note a distinct mosaic consisting of nanometer-sized CDW domains separated by sharp domain walls (c) Averaged STM spectroscopy  $dI/dV$  curves of the TaSse sample. The curves were collected at 1.2 K and 10 K, where the superconducting gap is fully open or fully closed, respectively. (d) STM spectroscopy  $dI/dV$  curves measured across the domain wall shown in the right part of this panel. The curves have been normalized and offset for clarity. The STM image was taken at 89 mV bias voltage and 94 pA tunneling current. The scale bar is 1 nm long.

perturbations, such as voltage pulses [34] or ultrafast laser pulses [35]. The complexity of electronic states at the nanometric scale is frequently encountered in strongly correlated systems [36] and can appear even when the Hamiltonian possesses the translational symmetry. It can emerge either because of quenched disorder [36,37] or frustration in the presence of long-range interactions [38,39]. In 1T-TaS<sub>2</sub> with polarons forming the triangular lattice, the effect of long-range Coulomb interactions close to the Mott transition may thus account for the observed mosaicity.

High resolution  $dI/dV$  measurements [Figs. 6(c) and 6(d)] performed both inside the domains and domain walls all show the opening of a superconducting gap,  $\Delta$ , in the density of states. While variations between different measurement points [Fig. 6(d)] were observed (most likely due to electronic state mosaicity [Fig. 6(b)]),  $\Delta$  was clearly visible in all. To avoid local variations, temperature dependent measurements were performed on a spatial  $5 \text{ nm} \times 5 \text{ nm}$  grid spanning two domains and a domain wall and then average curves were

taken in the same area [Fig. 6(c)].  $\Delta$  is clearly pronounced at 1.2 K and completely closed at 10 K. Despite the background variations in the  $dI/dV$  curves, we can still reliably estimate the average superconducting gap to be around  $\Delta \sim 1$  meV at 1.2 K with the variation of  $\Delta$  for about  $\pm 0.2$  meV between different points. This gives the average superconducting gap-to- $T_c$  ratio  $2\Delta/k_B T_c \approx 7$  and puts the Se-doped TaS<sub>2</sub> superconductor into a strong coupling limit.

#### IV. DISCUSSION

Present <sup>181</sup>Ta NQR and <sup>77</sup>Se NMR data provide some important constrains on the stability of the QSL and its rival states on the star-of-David triangular lattice of 1T-TaS<sub>2</sub>. The main experimental findings of this work can be summarized as: (i) the power-law dependence and a crossover to a low-temperature sublinear temperature dependence of  $1/T_1$  observed in <sup>181</sup>Ta NQR and <sup>77</sup>Se NMR for small Se doping, (ii) growth of intrinsic electronic inhomogeneities at low

temperatures, (iii) the collapse of the Mott-insulating QSL and the establishment of the metallic state characterized by the Korringa-type  $1/T_1$  with remnants of antiferromagnetic correlation effects for higher Se-doping levels, and (iv) the development of superconductivity with the large  $2\Delta/k_B T_c$  in highly Se-doped samples that develops from the inhomogeneous metallic state.

The power-law temperature dependence of  $1/T_1$  in general implies a gapless nonmagnetic state and has been in geometrically frustrated lattices taken as a fingerprint of the QSL [8,17–19]. Higher power-law exponents comply with the nodal type of QSL, while the sublinear  $T$  dependence of  $1/T_1$ , such as observed at low temperatures, has been argued to be a fingerprint of the QSL with a spinon Fermi surface [40]. In the latter case, the departure from the spinon-driven Korringa-like relaxation is due to the coupling of spinons with emergent gauge field fluctuations, which in the case of fractional spinon excitations give rise to the observed low-temperature sublinear dependence. However, the present study also shows that such power-law temperature dependencies of  $1/T_1$  survive when inhomogeneities in the form of domains in the electronic order [inset to Fig. 1(c)] are introduced on purpose in Se-doped samples indicating the initial robustness of the parent QSL at low Se-doping levels.

Local disorder is clearly present and manifested in the NQR and NMR parameters. There are two kinds of local disorder: the intrinsic structural distortions present already in the pristine 1T-TaS<sub>2</sub> and the Se-induced disorder in the doped samples. The additional broadening of <sup>181</sup>Ta NQR peaks in the doped samples is a direct measure of the latter. However, when Se randomly replaces S atom in TaS<sub>2</sub> layer, this has initially a surprisingly small effect on the spin dynamics in the QSL, as 1T-TaS<sub>2</sub> and 1T-TaS<sub>1.82</sub>Se<sub>0.18</sub> show qualitatively very similar  $1/T_1$  dependencies. On the other hand, the intrinsic structural distortions measured by the stretching exponent in spin-lattice relaxation data, are almost unaffected by the introduction of Se atoms into the lattice. They are thus likely an important intrinsic feature of the Mott state in the TaS<sub>2</sub> layer. Judging from the concomitant change in the  $1/T_1$  power laws and the decrease of  $p$  towards 0.5 (Fig. 3), it is this disorder that is strongly linked to the low-temperature spin dynamics. In a recent low-temperature STM study, two distinct types of orbitals were identified: a localized one concentrated at the central  $\alpha$  site and the more extended Wannier orbitals with the main weight along the edges of the star-of-David clusters [26]. It is thus tempting to propose that the observed intrinsic disorder reflects the orbital texturing within the TaS<sub>2</sub> layers. If this is indeed the case, then such orbital texturing will likely introduce some randomness in the exchange interactions as well, thus perturbing the ideal triangular  $S = 1/2$  lattice. The random-bond  $S = 1/2$  Heisenberg model on various frustrated 2D lattices, including the triangular lattice, has been recently extensively studied and reported to result in the gapless QSL-like state, which is best described as a random singlet state [21–23]. The ground state comprises nearly isolated singlet-dimers, clusters of resonating singlet-dimers, and orphan spins. Dynamical ‘liquidlike’ features originate from the excitations of the last two components and give rise to the  $T$ -linear low-temperature heat capacity and thermal conductivity and the almost constant susceptibility

followed by the intrinsic Curie-like tail at lower temperatures, which were observed also in 1T-TaS<sub>2</sub> [8,15,16,20]. If such a picture indeed applies to 1T-TaS<sub>2</sub>, then the increase in the low-temperature sublinear  $T$ -dependence of  $1/T_1$  for the 1T-TaS<sub>1.82</sub>Se<sub>0.18</sub> sample means that the density of states for itinerant spin-excitations increases with Se. Spatial variations in the density of states account for the broad distribution of nuclear spin-lattice relaxation rates clearly seen both in <sup>181</sup>Ta and <sup>77</sup>Se NMR. We also note that the itinerant nature of the spin excitations seems to rule out the alternative possibility of the valence-bond glass.

In a moderately doped material, such as 1T-TaS<sub>1.55</sub>Se<sub>0.45</sub>, the <sup>77</sup>Se spin-lattice relaxation dramatically changes in nature as it now approximately follows a Korringa relation <sup>77</sup>Se  $1/T_1 \propto T$  throughout a broad temperature interval. This is consistent with the metallic state where the spin-lattice relaxation is via itinerant charges and also supported by a large nearly temperature-independent shift of the <sup>77</sup>Se S peak [Fig. 4(a)]. Our observation of the metallicity at this Se-doping level is somewhat surprising, as previous resistivity studies on Se-doped TaS<sub>2</sub> showed a jump in the resistivity upon entering into the commensurate CDW phase and thus suggested that moderately doped compound should still be a Mott insulator [25]. This apparent inconsistency may arise from the fact that it is very difficult to prepare highly homogeneous samples upon Se doping as Se atoms can occupy also the interlayer space [Fig. 1(a)]. However, as this would decrease the effective Se doping even more it probably cannot explain the metallic <sup>77</sup>Se NMR shift and  $1/T_1$  in this part of the phase diagram. The growth of electronic mosaicity and the concomitant change in the orbital textures as suggested recently [26] in the constrained (but not yet fully percolated) interdomain walls [insets to Fig. 1(c)] could, on the other hand, explain the metallic-type <sup>77</sup>Se NMR response. Samples in this part of the phase diagram should thus be viewed as the samples showing large phase domain electronic inhomogeneities.

The shift of the metallic S peak is large and almost temperature independent. In general, the <sup>77</sup>Se NMR shift can be expressed as the sum of several contributions  $\delta = \delta_{cs} + \delta_{VV} + \delta_{iso}$ , where  $\delta_{cs}$  and  $\delta_{VV}$  are the chemical shift and the Van Vleck orbital term and  $\delta_{iso}$  is the isotropic Knight shift. The difference between the shifts of NS peak and S peak is due to  $\delta_{iso}$ , which is calculated to be  $\delta_{iso} = 1800$  ppm. For the layered transition-metal chalcogenides, one finds a typical value of  $d\delta_{iso}/d\chi_m = 16.8$  mol/emu [41], which allows us to estimate the Pauli susceptibility  $\chi_m = 1.1 \times 10^{-4}$  emu/mol and the corresponding density of states at the Fermi energy  $N(\epsilon_F) = 3.3$  states/eV. These values are by a factor of  $\sim 2$  larger than those of the high-temperature nearly commensurate CDW in pristine 1T-TaS<sub>2</sub> [8], which we attribute to the vicinity of the parent Mott insulating state. Further evidence for the importance of electron correlations can be derived from the modified Korringa relation [32]

$$\frac{1}{T_1 T \delta_{iso}^2} = \frac{4\pi k_B}{\hbar} \frac{\gamma_{77}^2}{\gamma_e^2} K_\alpha, \quad (3)$$

where  $\gamma_{77}$  and  $\gamma_e$  are the <sup>77</sup>Se and electron gyromagnetic ratios, respectively. The Korringa factor  $K_\alpha$  ranges from 0 to 1 and is a measure of the electron-electron interactions. Taking

the values for 1T-TaS<sub>2</sub>  $1/T_1T = 0.17 \text{ s}^{-1}\text{K}^{-1}$  and  $\delta_{\text{iso}} = 1800 \text{ ppm}$ , we calculate  $K_\alpha = 0.37$ , which is significantly less than 1 for the noncorrelated system. The reduced value of  $^{77}\text{Se}$   $1/T_1T$  picked up by  $K_\alpha$ , which on cooling suppresses by  $\sim 20\%$ , implies the presence of antiferromagnetic fluctuations that survive the Mottness collapse and are present even after the QSL is already destroyed. This may also explain the pronounced mosaicity at the nanometer scale in the electronic states, which are frequently encountered in the strongly correlated systems [36]. The observed superconductivity, which develops from such a state close to the Mott boundary and is characterized by a ratio  $2\Delta/k_B T_c \approx 7$ , should thus be discussed from this perspective. The situation is reminiscent of the families of unconventional superconductors, including cuprates or fullerides. More studies are needed to determine the symmetry of the superconducting order and to establish the role of electron correlations in the Cooper pairing.

In conclusion, we studied the effect of chemical pressure on QSL in 1T-TaS<sub>2</sub> induced by Se doping. Results clearly

underline the important role of antiferromagnetic fluctuations as well as electron correlations and disorder across the entire phase diagram. QSL appears surprisingly robust even when disorder increases with Se content. It is remarkable that the bulk superconductivity develops from a nanometre-mosaic electronic state. Although it is not clear from the present experimental data whether the observed superconductivity can be considered as a non-Bardeen-Cooper-Schrieffer or not, the unusually large  $2\Delta/k_B T_c \approx 7$  provides an important constraint on the nature of superconductivity.

#### ACKNOWLEDGMENTS

D.A. acknowledges financial support from the Slovenian Research Agency (Core Research Funding No. P1-0125 and Project No. J1-9145). M.v.M. and E.Z. acknowledge financial support from the Slovenian Research Agency (Core Research Funding No. P1-0099, Young Researcher PR-07586) and support of the CO Nanocenter.

- 
- [1] L. Balents, Spin liquids in frustrated magnets, *Nature (London)* **464**, 199 (2010).
- [2] X.-G. Wen, Quantum orders and symmetric spin liquids, *Phys. Rev. B* **65**, 165113 (2002).
- [3] Y. Shen, Y.-D. Li, H. Wo, Y. Li, S. Shen, B. Pan, Q. Wang, H.C. Walker, P. Steffens, M. Boehm *et al.*, Evidence for a spinon Fermi surface in a triangular-lattice quantum-spin-liquid candidate, *Nature (London)* **540**, 559 (2016).
- [4] J. A.M. Paddison, M. Daum, Z. Dun, G. Ehlers, Y. Liu, M. B. Stone, H. Zhou, and M. Mourigal, Continuous excitations of the triangular-lattice quantum spin liquid YbMgGaO<sub>4</sub>, *Nat. Phys.* **13**, 117 (2017).
- [5] T. Itou, A. Oyamada, S. Maegawa, M. Tamura, and R. Kato, Quantum spin liquid in the spin-1/2 triangular antiferromagnet EtMe<sub>3</sub>Sb[Pd(dmit)<sub>2</sub>]<sub>2</sub>, *Phys. Rev. B* **77**, 104413 (2008).
- [6] S. Ohira, Y. Shimizu, K. Kanoda, and G. Saito, Spin liquid state in  $\kappa$ -(BEDT-TTF)<sub>2</sub>Cu<sub>2</sub>(CN)<sub>3</sub> studied by muon spin relaxation method, *J. Low Temp. Phys.* **142**, 153 (2006).
- [7] K. T. Law and P. A. Lee, 1T-TaS<sub>2</sub> as a quantum spin liquid, *Proc. Natl. Acad. Sci. USA* **114**, 6996 (2017).
- [8] M. Klanjšek, A. Zorko, J. Mravlje, Z. Jagličič, P. K. Biswas, P. Prelovšek, D. Mihailovic, and D. Arčon, A high-temperature quantum spin liquid with polaron spins, *Nat. Phys.* **13**, 1130 (2017).
- [9] W.-Y. He, X. Y. Xu, G. Chen, K. T. Law, and P. A. Lee, Spinon Fermi surface in a cluster Mott Insulator Model on a Triangular Lattice and Possible Application to 1T-TaS<sub>2</sub>, *Phys. Rev. Lett.* **121**, 046401 (2018).
- [10] K. Rossnagel, On the origin of charge-density waves in select layered transition-metal dichalcogenides, *J. Phys.: Condens. Matter* **23**, 213001 (2011).
- [11] P. Fazekas and E. Tosatti, Electrical, structural and magnetic properties of pure and doped 1T-TaS<sub>2</sub>, *Philos. Mag. B* **39**, 229 (1979).
- [12] B. Sipoš, A. F. Kusmartseva, A. Akrap, H. Berger, L. Forró, and E. Tutiš, From Mott state to superconductivity in 1T-TaS<sub>2</sub>, *Nat. Mater.* **7**, 960 (2008).
- [13] D. Cho, Y.-H. Cho, S.-W. Cheong, K.-S. Kim, and H. W. Yeom, Interplay of electron-electron and electron-phonon interactions in the low-temperature phase of 1T-TaS<sub>2</sub>, *Phys. Rev. B* **92**, 085132 (2015).
- [14] S. Hellmann, T. Rohwer, M. Kalläne, K. Hanff, C. Sohrt, A. Stange, A. Carr, M. M. Murnane, H. C. Kapteyn, L. Kipp, M. Bauer, and K. Rossnagel, Time-domain classification of charge-density-wave insulators, *Nat. Commun.* **3**, 1069 (2012).
- [15] F. J. DiSalvo and J. V. Waszczak, Paramagnetic moments and localization in 1T-TaS<sub>2</sub>, *Phys. Rev. B* **22**, 4241 (1980).
- [16] A. Ribak, I. Silber, C. Baines, K. Chashka, Z. Salman, Y. Dagan, and A. Kanigel, Gapless excitations in the ground state of 1T-TaS<sub>2</sub>, *Phys. Rev. B* **96**, 195131 (2017).
- [17] T. Itou, A. Oyamada, S. Maegawa, and R. Kato, Instability of a quantum spin liquid in an organic triangular-lattice antiferromagnet, *Nat. Phys.* **6**, 673 (2010).
- [18] F. L. Pratt, P. J. Baker, S. J. Blundell, T. Lancaster, S. Ohira-Kawamura, C. Baines, Y. Shimizu, K. Kanoda, I. Watanabe, and G. Saito, Magnetic and non-magnetic phases of a quantum spin liquid, *Nature (London)* **471**, 612 (2011).
- [19] P. Khuntia, R. Kumar, A. V. Mahajan, M. Baenitz, and Y. Furukawa, Spin liquid state in the disordered triangular lattice Sc<sub>2</sub>Ga<sub>2</sub>CuO<sub>7</sub> revealed by NMR, *Phys. Rev. B* **93**, 140408(R) (2016).
- [20] H. Murayama, Y. Sato, T. Taniguchi, R. Kurihara, X. Z. Xing, W. Huang, S. Kasahara, Y. Kasahara, I. Kimchi, M. Yoshida, Y. Iwasa, Y. Mizukami, T. Shibauchi, M. Konczykowski, and Y. Matsuda, Coexisting localized and itinerant gapless excitations in a quantum spin liquid candidate 1T-TaS<sub>2</sub>, *Phys. Rev. Research* **2**, 013099 (2020).
- [21] H. Kawamura and K. Uematsu, Nature of the randomness-induced quantum spin liquids in two dimensions, *J. Phys.: Condens. Matter* **31**, 504003 (2019).
- [22] T. Shimokawa, K. Watanabe, and H. Kawamura, Static and dynamical spin correlations of the s=1/2 random-bond antiferromagnetic Heisenberg model on the triangular and kagome lattices, *Phys. Rev. B* **92**, 134407 (2015).



- [23] K. Watanabe, H. Kawamura, H. Nakano, and T. Sakai, Quantum spin-liquid behavior in the spin-1/2 random Heisenberg antiferromagnet on the triangular lattice, *J. Phys. Soc. Jpn.* **83**, 034714 (2014).
- [24] K. Riedl, R. Valenti, and S. M. Winter, Critical spin liquid versus valence-bond glass in a triangular-lattice organic antiferromagnet, *Nat. Commun.* **10**, 2561 (2019).
- [25] Y. Liu, R. Ang, W. J. Lu, W. H. Song, L. J. Li, and Y. P. Sun, Superconductivity induced by Se-doping in layered charge-density-wave system 1T-TaS<sub>2-x</sub>Se<sub>x</sub>, *Appl. Phys. Lett.* **102**, 192602 (2013).
- [26] S. Qiao, X. Li, N. Wang, W. Ruan, C. Ye, P. Cai, Z. Hao, H. Yao, X. Chen, J. Wu, Y. Wang, and Z. Liu, Mottness Collapse in 1T-TaS<sub>2-x</sub>Se<sub>x</sub> Transition-Metal Dichalcogenide: An Interplay between Localized and Itinerant Orbitals, *Phys. Rev. X* **7**, 041054 (2017).
- [27] L. J. Li, W. J. Lu, X. D. Zhu, L. S. Ling, Z. Qu, and Y. P. Sun, Fe-doping-induced superconductivity in the charge-density-wave system 1T-TaS<sub>2</sub>, *EPL (Europhysics Letters)* **97**, 67005 (2012).
- [28] M. Naito, H. Nishihara, and S. Tanaka, Nuclear quadrupole resonance in the charge density wave state of 1T-TaS<sub>2</sub>, *J. Phys. Soc. Jpn.* **53**, 1610 (1984).
- [29] M. Naito, H. Nishihara, and S. Tanaka, NMR study of <sup>181</sup>Ta in the commensurate charge density wave state of 1T-TaSe<sub>2</sub> and 1T-TaS<sub>2</sub>, *J. Phys. C: Solid State* **16**, L387 (1983).
- [30] H. Dudder, Introduction to Selenium-77 NMR and list of abbreviations, in *Chemical Shifts and Coupling Constants for Selenium-77* (Springer, Berlin, Heidelberg, 2004), pp. 1–11.
- [31] C. P. Slichter, *Principles of Magnetic Resonance* (Springer, Berlin, Heidelberg, 2013).
- [32] R. E. Walstedt, *The NMR Probe of High-Tc Materials*, Vol. 228 (Springer, Berlin, Heidelberg, 2008).
- [33] H. Xiao, T. Hu, A. P. Dioguardi, N. apRoberts Warren, A. C. Shockley, J. Crocker, D. M. Nisson, Z. Viskadourakis, X. Tee, I. Radulov, C. C. Almasan, N. J. Curro, and C. Panagopoulos, Evidence for filamentary superconductivity nucleated at antiphase domain walls in antiferromagnetic CaFe<sub>2</sub>As<sub>2</sub>, *Phys. Rev. B* **85**, 024530 (2012).
- [34] L. Ma, C. Ye, Y. Yu, X. Fang Lu, X. Niu, S. Kim, D. Feng, D. Tomanek, Y.-W. Son, X. Hui Chen, and Y. Zhang, A metallic mosaic phase and the origin of Mott-insulating state in 1T-TaS<sub>2</sub>, *Nat. Commun.* **7**, 10956 (2016).
- [35] L. Stojchevska, I. Vaskivskiy, T. Mertelj, P. Kusar, D. Svetin, S. Brazovskii, and D. Mihailovic, Ultrafast switching to a stable hidden quantum state in an electronic crystal, *Science* **344**, 177 (2014).
- [36] E. Dagotto, Complexity in strongly correlated electronic systems, *Science* **309**, 257 (2005).
- [37] V. B. Shenoy, D. D. Sarma, and C. N. R. Rao, Electronic phase separation in correlated oxides: the phenomenon, its present status and future prospects, *ChemPhysChem* **7**, 2053 (2006).
- [38] A. Zorko, O. Adamopoulos, M. Komelj, D. Arčon, and A. Lappas, Frustration-induced nanometre-scale inhomogeneity in a triangular antiferromagnet, *Nat. Commun.* **5**, 3222 (2014).
- [39] M. Pregelj, A. Zorko, O. Zaharko, H. Nojiri, H. Berger, L.C. Chapon, and D. Arčon, Spin-stripe phase in a frustrated zigzag spin-1/2 chain, *Nat. Commun.* **6**, 7255 (2015).
- [40] M. Gomilšek, M. Klanjšek, R. Žitko, M. Pregelj, F. Bert, P. Mendels, Y. Li, Q.M. Zhang, and A. Zorko, Field-Induced Instability of a Gapless Spin Liquid with a Spinon Fermi Surface, *Phys. Rev. Lett.* **119**, 137205 (2017).
- [41] R. Dupree, W. W. Warren, and F. J. DiSalvo, <sup>77</sup>Se NMR study of the electronic instability in TiSe<sub>2</sub>, *Phys. Rev. B* **16**, 1001 (1977).